2001

A New Compensating Element for a Femtosecond Photoelectron Gun

Bao-Liang Qian
Old Dominion University

Hani E. Elsayed-Ali
Old Dominion University, helsayed@odu.edu

Original Publication Citation

Qian, B. L., & Elsayed-Ali, H. E. (2001). A new compensating element for a femtosecond photoelectron gun. *Review of Scientific Instruments, 72*(9), 3507-3513. doi:10.1063/1.1387254

A new compensating element for a femtosecond photoelectron gun

Bao-Liang Qian
Department of Electrical and Computer Engineering and the Applied Research Center, Old Dominion University, Norfolk, Virginia 23529-0256 and Department of Applied Physics, National University of Defense Technology, Changsha 410073, Hunan, People's Republic of China

Hani E. Elsayed-Ali[a)]
Department of Electrical and Computer Engineering and the Applied Research Center, Old Dominion University, Norfolk, Virginia 23529-0256

(Received 14 March 2001; accepted for publication 16 May 2001)

Design and analysis of a new compensating element for improving the electron pulse front and compressing the pulse duration in a femtosecond photoelectron gun are described. The compensating element is a small metallic cylindrical cavity in which an external voltage is applied in such a way that a special electric field forms and interacts with the electron pulse. This electric field reduces the distances between the faster and slower electrons inside the cavity and efficiently compensates for electron pulse broadening caused by the photoelectron energy spread and space charge effects. Poisson's equation and the equation of motion are solved to obtain the electron trajectories. Results highlight the important design parameters of the new compensating element and show its feasibility in compressing electron pulses in the femtosecond regime. © *2001 American Institute of Physics.* [DOI: 10.1063/1.1387254]

I. INTRODUCTION

Motivated by the need to improve the temporal resolution of streak cameras[1–15] and time resolved electron diffraction,[16–34] the development of photoelectron guns capable of delivering picosecond and subpicosecond electron pulses has been investigated extensively. However, the technology for generating electron pulses with pulse widths of ~ 100 fs, electron energies of 10–50 keV with electron energy spread in the few eV range, and 10^3 to 10^4 electrons per pulse are still under development. The main obstacles are photoelectron energy spread and space charge effects that cause significant electron pulse broadening.

In Ref. 35, relativistic electron pulses 50 fs in duration, 2.6 MeV electron energy, with $(2-4.6)\times 10^8$ electrons per pulse were obtained experimentally using an electron pulse compression technology based on introducing a large energy spread followed by a magnetic prism. However, for applications in streak cameras and electron diffraction, the electron energy is far below the relativistic regime and has a few eV or less energy spread. This makes magnetic electron pulse compression, as applied to a relativistic electron pulse with energy spread in the keV range, unfeasible. A method of temporal dispersion compression was also suggested for the nonrelativistic case to produce 50 fs electron pulses, but to our knowledge, has not been experimentally implemented.[9,10] The effects of electron energy spread on electron pulse broadening can be reduced, to some extent, in the photocathode-to-mesh region by choosing a photocathode with a suitable work function, close to the laser photon energy, and applying a relatively high acceleration electric field in the vicinity of the photocathode.[2,4,14] On the contrary, space charge effects causing electron pulse broadening are more difficult to remove. Electron pulse broadening is often larger in the electron drift region than in the photocathode-to-mesh region.[3,5,36–38] For a photoactivated electron gun activated by a femtosecond laser pulse, the electron pulse broadens into the picosecond range in a short time as it propagates towards the anode and in the postanode drift region. For the photoelectron gun configuration shown in Fig. 1(a) we have developed a simple fluid model to investigate the electron pulse broadening caused by photoelectron energy spread and space charge effects in the photocathode-to-anode region and in the postanode drift region.[39] Pulse broadening due to the initial photoelectron energy spread occurs mainly in the photocathode-to-anode region and is estimated to be ~ 150 fs for an initial photoelectron energy spread $\Delta E_0 = 0.2$ eV, $d = 3$ mm, and $V_0 = 30$ kV, where d is the photocathode-to-anode mesh spacing and V_0 is voltage applied to the photocathode with the anode grounded, as shown in Fig. 1(a). However, pulse broadening due to space charge effects becomes severe in the postanode drift region, when the electron density is high, because of the large drift time in that region. Pulse broadening due to space charge effects in the postanode drift region can be expressed as[39]

$$\Delta t_{\mathrm{sp}} = \frac{e^{1/2} m^{1/2} L^2 N}{4\sqrt{2}\,\pi V_0^{3/2} \varepsilon_0 r_b^2}, \tag{1}$$

where $-e$ and m are the charge and mass of an electron, V_0 is the voltage applied between the cathode and the anode (mesh), r_b is the radius of the electron beam, L is the length of the drift region, N is the number of the electrons contained in the electron pulse, and ε_0 is the vacuum permittivity. Δt_{sp} is calculated to be 350 fs for $L = 40$ cm, $N = 1000$, r_b

a)Author to whom correspondence should be addressed; electronic mail: helsayed@odu.edu

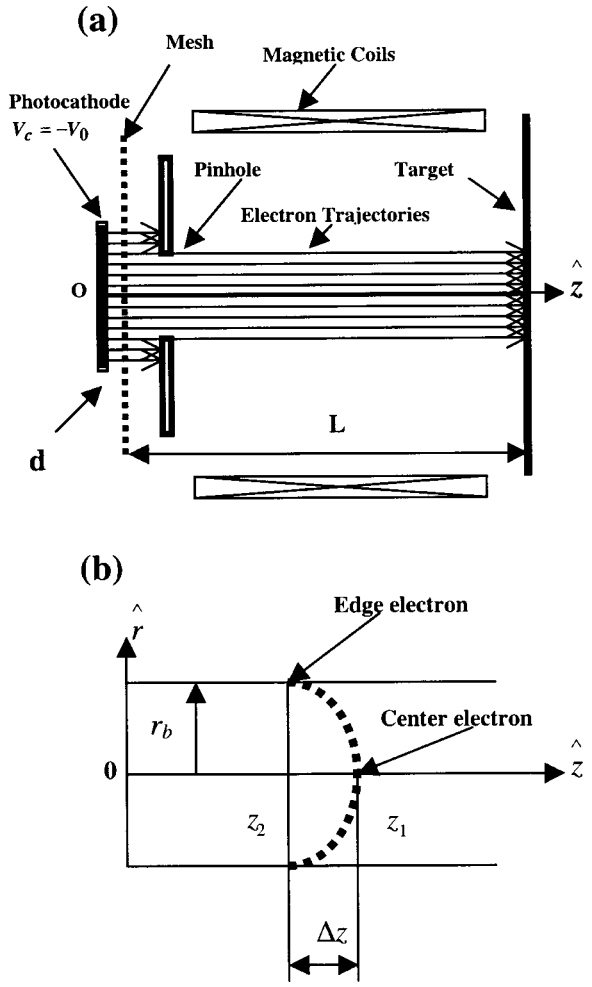

FIG. 1. (a) The configuration of a photoelectron gun with magnetic lens. (b) A typical electron pulse front due to electron beam divergence caused by space charge effects and the initial electron energy spread.

$=0.45$ mm, and $V_0=30$ kV. Additional electron pulse broadening occurs due to the energy spread of the photoelectrons at the surface of the photocathode. For a laser pulse of $\tau_0=50$ fs in duration and electron pulse broadening $\Delta t_e \approx 150$ fs due to initial photoelectron energy spread, the electron pulse width will be $\Delta t_p=\tau_0+\Delta t_e+\Delta t_{sp}\approx 550$ fs, assuming a square pulse shape to allow for obtaining an analytical solution. Therefore to construct an electron gun capable of delivering 1000 electrons per pulse over a 40 cm drift distance, with a pulse width less than 200 fs, it is necessary to develop an efficient compensating device for compressing an electron pulse broadened by space charge effects and the initial photoelectron energy spread. This compensating device can also be applied to achieve shorter electron pulses, if the drift distance is reduced.

In general, an electron traveling exactly along the center axis will spend less time than an electron traveling off-axially.[9] Electron beam divergence in the E-field free drift region is mainly caused by the electron space charge effects and energy spread. The electron pulse front resembles the shape shown in Fig. 1(b). In this case, the space charge effects of the inner electrons in the electron pulse increase the radial components of velocities of the edge electrons and lead to divergence of the electron beam. Similarly, an electron traveling along the center of the pulse front is faster along the axial direction than other electrons because it is accelerated by the space charge of the electrons following it. Consequently, for edge electrons the axial components of velocities are lower than for electrons at or near the center that are drifting only along the axial direction. Therefore if an axially directed acceleration electric field that increases off-axially, or an axially directed decelerating electric field that decreases off-axially, is generated in the drift region, the axial distances between the center electron and the edge electrons will be decreased. Thus the electron pulse front can be improved and the temporal dispersion of the electron gun can be reduced. The purpose of this article is to introduce a new electron dispersion-compensating element for application in femtosecond photoelectron guns. Our results show that this compensating element is efficient in compressing a femtosecond electron pulse.

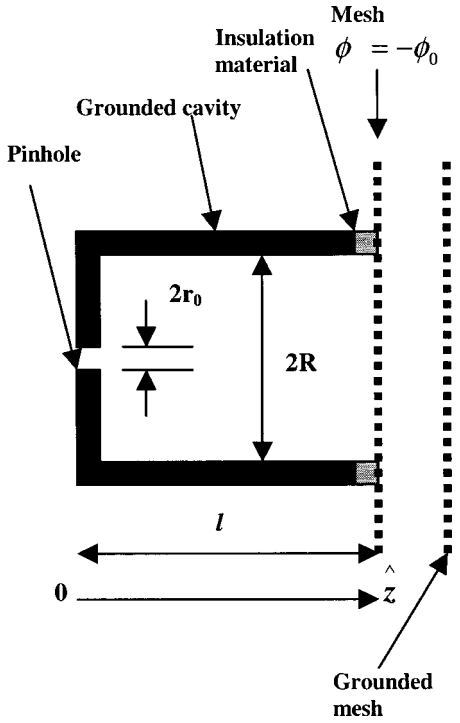

FIG. 2. The configuration of the compensating cavity for a femtosecond electron gun.

The remainder of the present article is as follows. In Sec. II the configuration of the compensating element and the basic formulation are given. In Sec. III the equation of motion is solved to obtain the trajectories of the electrons in an electron pulse front and the results are given showing the compression of the electron pulse.

II. CONFIGURATION AND MODEL OF THE COMPENSATING ELEMENT

The basic configuration of the compensating element is shown in Fig. 2. The element is a metallic cylindrical cavity with a length l and a radius R. On one side of the cavity there is a pinhole through which the electron pulse can pass along the axial direction $\hat{z}$, and on the opposite side there is a fine mesh that is electrically insulated from the other sides

of the cavity by an insulation material or vacuum. The thickness of the insulation material or vacuum gap should be much smaller than the length l of the cavity. In addition, the radius of the pinhole r_0 is assumed to be much smaller than that of the cavity. The cavity is grounded except for the mesh, which has an applied potential of $\phi=-\phi_0<0$. Just after this fine mesh there is another fine mesh that is grounded and used to form a relatively uniform acceleration electric field for electrons exiting from the compensating cavity. This grounded mesh gives a relatively uniform acceleration to the electrons after the compensating element and shields the electric field produced by the fine mesh at a potential $\phi=-\phi_0<0$, allowing the electron pulse to subsequently drift in an electric field free region. We discuss the interaction of the electron pulse with the electric field inside the cavity.

The potential distribution ϕ within the cavity can be described by Poisson's equation in the cylindrical coordinates (r,θ,z), which is written as

$$\frac{1}{r}\frac{\partial}{\partial r}\left(r\frac{\partial\phi}{\partial r}\right)+\frac{\partial^2\phi}{\partial z^2}=0, \tag{2}$$

where $\partial/\partial\theta=0$ because of the azimuthal symmetry. The fine mesh at $\phi=-\phi_0<0$ is treated as a solid metallic sheet, and the effects of the isolation material and the pinhole whose radius r_0 is much smaller than the radius R of the cavity are ignored. Solving Eq. (2) using the boundary conditions of $\phi(r=R)=\phi(z=0)=0$ and $\phi(z=l)=-\phi_0<0$, one can obtain the potential distribution ϕ, which is written as

$$\phi=-\sum_{n=1}^{\infty}\frac{2\phi_0}{\alpha_n J_1(\alpha_n)}\frac{\sinh\left(\frac{\alpha_n z}{R}\right)}{\sinh\left(\frac{\alpha_n l}{R}\right)}J_0\left(\frac{\alpha_n r}{R}\right), \tag{3}$$

and the components of the electric field in the cavity are expressed as

$$E_r=-\frac{\partial\phi}{\partial r}=-\sum_{n=1}^{\infty}\frac{2\phi_0}{RJ_1(\alpha_n)}\frac{\sinh\left(\frac{\alpha_n z}{R}\right)}{\sinh\left(\frac{\alpha_n l}{R}\right)}J_1\left(\frac{\alpha_n r}{R}\right) \tag{4}$$

and

$$E_z=-\frac{\partial\phi}{\partial z}=\sum_{n=1}^{\infty}\frac{2\phi_0}{RJ_1(\alpha_n)}\frac{\cosh\left(\frac{\alpha_n z}{R}\right)}{\sinh\left(\frac{\alpha_n l}{R}\right)}J_0\left(\frac{\alpha_n r}{R}\right), \tag{5}$$

where E_r is the radial component of the electric field, E_z is the axial component of the electric field, α_n is the nth root of the zero-order Bessel function $J_0(x)$, satisfying $J_0(\alpha_n)=0$, and $J_1(x)$ is the first-order Bessel function.

It can be seen that the axial electric field $E_z>0$, thus all the electrons that experience this field will be decelerated. The axial component E_z of the electric field decreases with increasing r due to the property of the Bessel function $J_0(x)$ and thus this field can be a compensating field. In this case, the center electrons in the electron pulse will be decelerated more than the edge electrons, which can improve the pulse front and compress the electron pulse. The compensating element described in Fig. 2 should be immersed in a relatively strong axial guide magnetic field B to compensate for the divergence due to E_r. The parameters of ϕ_0, l, and R can be adjusted in order to achieve the desired compensation. Equations (4) and (5) are evaluated numerically to obtain the distribution of the electric field in the cavity. For the sake of convenience, dimensionless variables are used in the calculations. These normalization variables are $E_0=2\phi_0/R$ and $r_c=mc/eB$, where c is the speed of light in vacuum and B is the constant axial magnetic field applied in the compensating cavity.

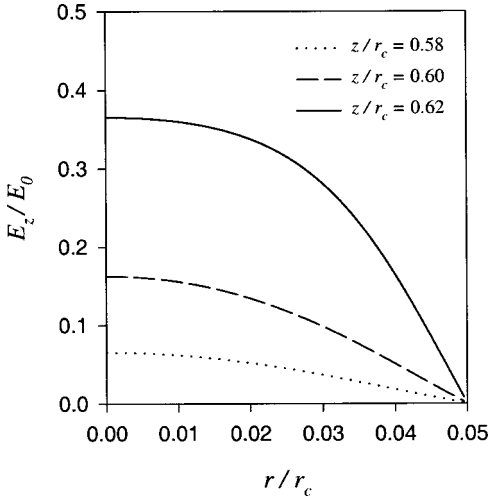

FIG. 3. The axial electric field E_z in the compensating cavity as a function of r for $R/r_c=0.05$ and $l/r_c=0.65$ in the cases of $z/r_c=0.58$, 0.60, and 0.62.

Figure 3 shows the axial electric field E_z as a function of the distance r from the center of the cylindrical cavity for $R/r_c=0.05$ and $l/r_c=0.65$ in the cases of $z/r_c=0.58$, 0.60, and 0.62. We can see from Fig. 3 that E_z decreases with the increase of r and increases with z under the condition that z is not too close to l. Detailed calculations (results not shown in Fig. 3) indicate that the dependence of E_z on r will change when z is very close to l due to $J_1(\alpha_n)$ appearing in the denominators of Eqs. (4) and (5). It is shown later that this will not affect the performance of the cavity in improving the electron pulse front and compressing the pulse width of the photoelectron gun because this region is too small to alter the compressing function of the cavity. Figure 4 shows the radial electric field E_r as a function of r for $R/r_c=0.05$ and $l/r_c=0.65$ in the cases of $z/r_c=0.58$, 0.60, and 0.62. As can be seen from Fig. 4, the absolute value $|E_r|$ of the radial electric field first increases with both r and z, but then decreases with r as r becomes very close to R. The divergence effects of E_r on the electron pulse can be efficiently compensated for by the axial magnetic field B. In addition, one can also observe that the center electron of the electron pulse front will lose more kinetic energy than the edge electrons because the absolute value $|\phi|$ of the potential decreases as r increases according to Eq. (3).

An efficient way to investigate the physics of the compensating element is to depict the trajectories of the electrons

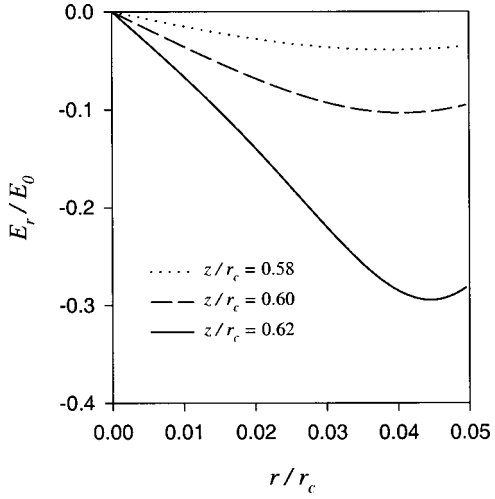

FIG. 4. The radial electric field E_r in the compensating cavity as a function r for $R/r_c=0.05$ and $l/r_c=0.65$ in the cases of $z/r_c=0.58$, 0.60, and 0.62.

contained in the electron pulse front when the pulse passes through the element. We next formulate a model by which the electron trajectories of the electron pulse front can be obtained. It is appropriate to assume that the length l of the compensating cavity is short enough to neglect the self-space charge effects of the electron beam.[39] In this case, the motion of the electrons will be only in the externally applied constant magnetic field B and the electric field $\mathbf{E}=E_r\hat{r}+E_z\hat{z}$ in the compensating cavity, which is given by Eqs. (4) and (5). The components of the equation of motion for an electron are written as

$$\frac{dv_r}{dt}=\frac{v_\theta^2}{r}-\frac{e}{m}[E_r+v_\theta B], \tag{6}$$

$$\frac{dv_\theta}{dt}=\frac{eBv_r}{m}-\frac{v_r v_\theta}{r}, \tag{7}$$

and

$$\frac{dv_z}{dt}=-\frac{eE_z}{m}, \tag{8}$$

where $-e$ and m are electron charge and mass, $\mathbf{v}=v_r\hat{r}+v_\theta\hat{\theta}+v_z\hat{z}$ is the electron velocity in cylindrical coordinates, and E_r and E_z are given by Eqs. (4) and (5). Other useful relations are

$$\frac{dr}{dt}=v_r, \tag{9}$$

$$\frac{d\theta}{dt}=\frac{v_\theta}{r}, \tag{10}$$

and

$$\frac{dz}{dt}=v_z. \tag{11}$$

Equations (6)–(11) can be used to investigate the motion of the electrons in the compensating cavity. There are no analytical solutions to Eqs. (6)–(11), and numerical solutions are necessary to obtain the electron trajectories.

III. NUMERICAL RESULTS AND DISCUSSIONS

In this section we numerically solve Eqs. (6)–(11) to further explore the physics of the compensating element described in Fig. 2. We assume that the electron pulse is azimuthally symmetric. Therefore all the edge electrons in the electron front have the same velocity and trajectory. We only consider two kinds of electrons contained in the electron pulse front, i.e., the center electron and the edge electrons. It is convenient to use dimensionless variables to treat these equations. As shown in Fig. 1(b), in addition to $r_c=mc/eB$ and $E_0=2\phi_0/R$, the physical quantities involved in the following numerical results are the radius r_b of the electron beam or the radial position $r=r_b$ of the edge electrons in the electron pulse front, the radial position $r=r_{\mathrm{cen}}=0$ of the center electron, the axial position $z=z_1$ and axial velocity $v_z=v_{z1}$ of the center electron, the axial position $z=z_2$ and axial velocity $v_z=v_{z2}$ of the edge electrons, the axial distance $\Delta z=z_1-z_2$ and the axial velocity difference $\Delta v_z=v_{z1}-v_{z2}$ between the center electron and the edge electrons, the average initial drift velocity v_0 of the electrons at the entrance of the compensating cavity, the average initial kinetic energy $\varepsilon=mv_0^2/2$ of the electrons, the initial electron energy spread $\Delta\varepsilon$ of the electron pulse at the entrance of the cavity, and the cyclotron frequency $\omega_c=eB/m$ of the electrons in the magnetic field B.

In addition, at the entrance of the compensating cavity, the center electron is initially at $(r,z)=(r_{\mathrm{cen}},z_1)=(0,z_{10})$ with $z_{10}>0$, and the edge electrons are initially at $(r,z)=(r_b,z_2)=(r_b,z_{20})=(r_b,0)$. Therefore the axial distance between the center electron and the edge electrons is initially $\Delta z=\Delta z_0=z_{10}$. The radius r_0 of the pinhole at the entrance of the compensating cavity is assumed to be larger than the initial beam radius r_b. At the axial position $z=l$, the electron reaches the end of the compensating cavity. In order to show the effects of electron energy spread on the electron pulse front, we will investigate the case in which the initial kinetic energy difference between the center electron and the edge electrons at the entrance of the compensating cavity is equal to the energy spread $\Delta\varepsilon$. Moreover, the initial velocity $\mathbf{v}_0$ of the electrons at the entrance of the compensating cavity takes the form of $\mathbf{v}_0=v_0[\sin(\theta_0)\hat{r}+\cos(\theta_0)\hat{z}]$, where θ_0 is the velocity divergence angle. The center electron is assumed to have $\theta_0=\theta_{01}=0$, but for the edge electrons $\theta_0=\theta_{02}>0$, where θ_{01} and θ_{02} refer to the velocity divergence angles of center electron and edge electrons, respectively. It is worth noting that our model does not include the details of the shape of the electron pulse front and the initial axial distance Δz_0 between the center electron and the edge electrons depends on the electron dynamics before the entrance of the compensating cavity.

Figure 5 shows the radial position r of the edge electrons in the electron pulse front as a function of the axial position z for $r_b/r_c=0.0075$, $z_{20}=0$, $v_0/c=1/3$, $R/r_c=0.05$, $l/r_c=0.65$, and $E_0/cB=1.1$ in the cases of $\theta_{02}=0$ and $\theta_{02}=0.016$. It can be seen from Fig. 5 that the beam radius r_b varies from 0.0075 r_c to about 0.0164 r_c in the case of $\theta_{02}=0.016$ when the electron pulse passes through the compensating element. However, the beam radius r_b changes from

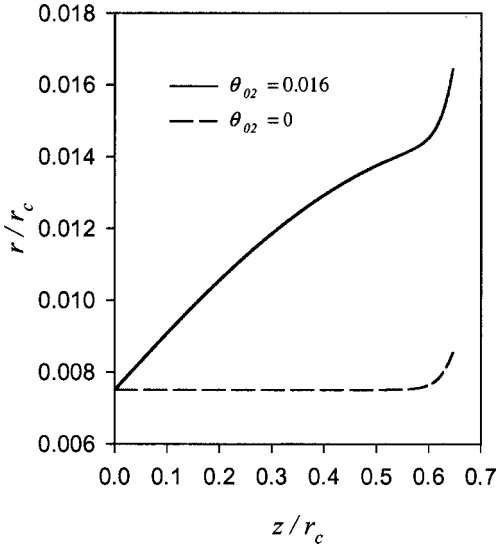

FIG. 5. The radial position r of the edge electrons in the electron pulse front as a function of axial position z for $r_b/r_c=0.0075$, $z_{20}=0$, $v_0/c=1/3$, $R/r_c=0.05$, $l/r_c=0.65$, and $E_0/cB=1.1$ in the cases of $\theta_{02}=0$ and $\theta_{02}=0.016$.

0.0075 r_c to about 0.0085 r_c in the case of $\theta_{02}=0$. Therefore the variation of the beam radius is mainly due to the initial electron velocity divergence represented by the value of θ_{02}. The effect of the radial electric field E_r on the beam divergence is small in the case of a constant axial applied magnetic field B. The value of E_r is very small near $r=0$ according to Fig. 4, and therefore its divergence effect is negligible.

Figure 6 shows the axial velocities v_z of the center electron and edge electrons in the electron pulse front as a function of z for $r_b/r_c=0.0075$, $z_{10}/r_c=0.000\,40$, $z_{20}=0$, $\theta_{01}=0$, $\theta_{02}=0.016$, $v_0/c=1/3$, $\Delta\varepsilon/\varepsilon=0.000\,036$, $R/r_c=0.05$, $l/r_c=0.65$, and $E_0/cB=1.1$. Figure 6 indicates that the axial velocities of the center electron and edge electrons are decreased as the electron pulse reaches the end of the

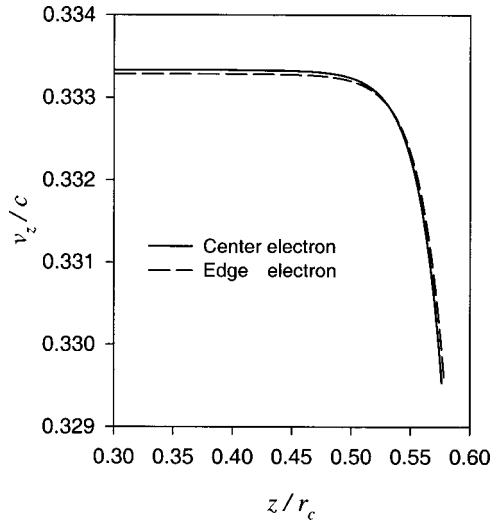

FIG. 6. The axial velocities v_z of the center electron and edge electrons in the electron pulse front as a function of z for $r_b/r_c=0.0075$, $z_{10}/r_c=0.000\,40$, $z_{20}=0$, $\theta_{01}=0$, $\theta_{02}=0.016$, $v_0/c=1/3$, $\Delta\varepsilon/\varepsilon=0.000\,036$, $R/r_c=0.05$, $l/r_c=0.65$, and $E_0/cB=1.1$.

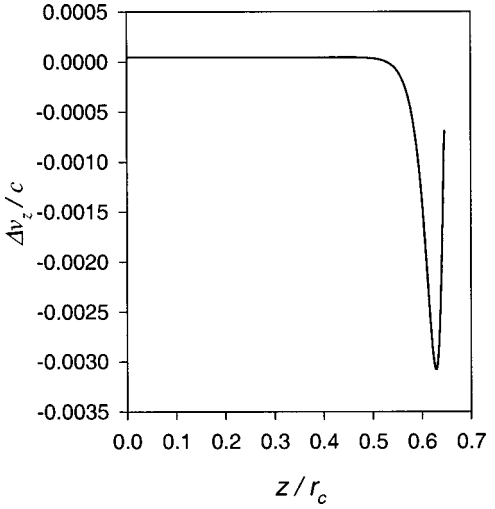

FIG. 7. The axial velocity difference $\Delta v_z=v_{z1}-v_{z2}$ between the center electron and edge electrons in the electron pulse front as a function of z for $r_b/r_c=0.0075$, $z_{10}/r_c=0.000\,40$, $z_{20}=0$, $\theta_{01}=0$, $\theta_{02}=0.016$, $v_0/c=1/3$, $\Delta\varepsilon/\varepsilon=0.000\,036$, $R/r_c=0.05$, $l/r_c=0.65$, and $E_0/cB=1.1$.

compensating cavity. In addition, as shown in Fig. 6, the axial velocity of the edge electrons is slightly lower than that of the center electron at the entrance of the compensating cavity. However, the edge electrons catch up with the center electron because their axial velocity is brought slightly larger than that of the center electron near the exit of the compensating cavity. Thus the compensating electric field in the cavity causes pulse compression. The compensating effect can be also clearly seen from Fig. 7, where we have plotted the axial velocity difference $\Delta v_z=v_{z1}-v_{z2}$ between the center electron and the edge electrons in the electron pulse front as a function of z for the same parameters used in Fig. 6. At the entrance of the cavity, the velocity of the center electron is larger than the velocity of the edge electrons, $\Delta v_z=v_{z1}-v_{z2}>0$. However, for $z/r_c>0.53$, $\Delta v_z<0$ and the edge electrons will become faster than the center electron after the interaction of the electron pulse with the compensating electric field in the cavity. It is interesting to note that the magnitude of Δv_z first increases and then decreases with z in the region $0.53<z/r_c<0.65$. This occurs because the field E_z depends on r such that it decelerates the center electron more than the edge electrons over most of the cavity length, however, near the end of the compensating cavity this dependence of E_z on r is reversed. For $0.53<z/r_c<0.65$, $\Delta v_z<0$ indicating that the compensating function of the cavity is still maintained in spite of the variation of Δv_z near the end of the compensating cavity.

The improvement in the electron front and compression of the electron pulse can be observed in Fig. 8, where we have plotted the axial distance $\Delta z=z_1-z_2$ between the center electron and the edge electrons in the electron pulse front as a function of time t for $r_b/r_c=0.0075$, $\theta_{01}=0$, $\theta_{02}=0.016$, $v_0/c=1/3$, $\Delta\varepsilon/\varepsilon=0.000\,036$, $R/r_c=0.05$, $l/r_c=0.65$, and $E_0/cB=1.1$ in the cases of different initial axial distances of $\Delta z_0/r_c=0.000\,45$, $0.000\,40$, and $0.000\,35$. As can be seen from Fig. 8, the axial distance between the center electron and the edge electrons first increases with time t due to initial energy spread and beam divergence, but then de-

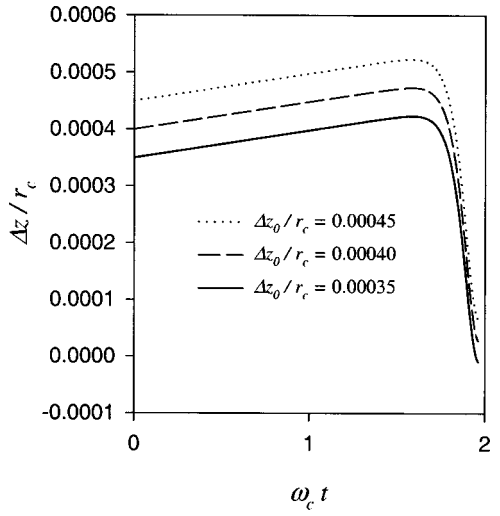

FIG. 8. The axial distance $\Delta z = z_1 - z_2$ between the center electron and the edge electrons in the electron pulse front as a function of time t for $r_b/r_c = 0.0075$, $\theta_{01} = 0$, $\theta_{02} = 0.016$, $v_0/c = 1/3$, $\Delta\varepsilon/\varepsilon = 0.000\,036$, $R/r_c = 0.05$, $l/r_c = 0.65$, and $E_0/cB = 1.1$ in the cases of different initial axial distances of $\Delta z_0/r_c = 0.000\,45$, $0.000\,40$, and $0.000\,35$.

creases abruptly with time t due to the strong compensating electric field experienced by the electron pulse in the cavity. This is easily understood using the data shown in Figs. 6 and 7, where the curves indicate the change of sign of the axial velocity difference Δv_z between the center electron and the edge electrons. As shown in Fig. 8, the value of Δz in the case of $\Delta z_0/r_c = 0.000\,35$ can even become negative as the time t increases, which means that the edge electrons have completely caught up with the center electron, and consequently the electron pulse duration is compressed.

The design of the compensating cavity can be based on the numerical results obtained above. However, a long compensating device should be avoided because a long electron beam drift distance will result in a considerable electron pulse broadening due to space charge effects. A compensating cavity of less than 6 cm in length is suitable for a 200 fs electron gun with 10^3 electrons per pulse because in this case the space charge pulse broadening Δt_{sp} in the 6-cm cavity is less than 10 fs for a beam radius of $r_b = 0.45$ mm and the average electron drift kinetic energy at the cavity entrance of $\varepsilon = 30$ keV according to Eq. (1). In addition, the radius of the compensating cavity should also be as small as possible in order to focus the distribution of the electric field to meet the compensating requirements inside the cavity. The results shown in Figs. 5–8 indicate that the appropriate design parameters of the compensating cavity can be $l = 5.6$ cm, $R = 0.4$ cm, $\phi_0 = 14$ kV, and $B = 200$ G. These design parameters apply for a photoelectron gun with an electron energy of 30 keV, a space charge-caused electron energy spread of less than 1.1 eV, an electron beam radius ~ 0.6 mm at the compensating cavity, and 10^3 electrons per pulse. In the example we gave earlier, a 50 fs photoelectron pulse at the photocathode broadened by its energy spread and space charge effects over a 40 cm drift distance to $\Delta t_p \approx 550$ fs.[39] For these design parameters, the electron pulse front can be improved considerably and the electron pulse duration can be reduced by as much as $\Delta z_0/v_0 \approx 350$ fs according to Fig. 8. In this case, the electron pulse duration may reach a value of 200 fs ($= 550 - 350$ fs) under the condition that the shape of the electron pulse front, with a value of Δz_0 due to space charge effects, is the major factor that affects the electron pulse duration. The gap length between the mesh with potential $\phi_0 = 14$ kV and the end of the 5.6 cm cavity can be a few mm, enough to hold-off breakdown in vacuum. The model ignores this distance, which is valid when the length of the cavity is much larger than the width of the insolation gap.

This new compensating element can be used to extend the temporal resolution of streak cameras and time-resolved electron diffraction. Depending on the design parameters and the shape of the electron pulse, for a femtosecond electron gun with an electron energy of 30 keV and 10^3 electrons per pulse, the electron pulse duration can be reduced by 350 fs when using a single compensating cavity with a radius of 0.4 cm and 5.6 cm in length.

ACKNOWLEDGMENTS

This work was supported by the National Science Foundation, Grant No. DMR-9988669, the U.S. Department of Energy Grant No. DE-FG02-97ER45625, and a grant from the Jeffress Foundation. The research by B.-L. Qian was supported by the abroad-studying funds from the National University of Defense Technology in the People's Republic of China.

[1] D. J. Bradley and W. Sibbett, Appl. Phys. Lett. **27**, 382 (1975).
[2] V. N. Platonov and M. Ya. Shchelev, Sov. Phys. Tech. Phys. **24**, 954 (1979).
[3] H. Niu and W. Sibbett, Rev. Sci. Instrum. **52**, 1830 (1981).
[4] H. Niu, W. Sibbett, and M. R. Baggs, Rev. Sci. Instrum. **53**, 563 (1982).
[5] W. Sibbett, H. Niu, and M. R. Baggs, Rev. Sci. Instrum. **53**, 758 (1982).
[6] K. Kinoshita, M. Ito, and Y. Suzuki, Rev. Sci. Instrum. **58**, 932 (1987).
[7] A. Finch, Y. Liu, H. Niu, W. Sibbett, W. E. Slent, D. R. Walker, Q. L. Yang, and H. Zhang, Proc. SPIE **1032**, 622 (1988).
[8] J. Ihlemann, A. Helmbold, and H. Staerk, Rev. Sci. Instrum. **59**, 2502 (1988).
[9] H. Niu, V. P. Degtyareva, V. N. Platonov, A. M. Prokhorov, and M. Ya. Schelev, Proc. SPIE **1032**, 79 (1988).
[10] H. Niu, H. Zhang, Q. L. Yang, Y. P. Liu, Y. C. Wang, Y. A. Reng, and J. L. Zhou, Proc. SPIE **1032**, 472 (1988).
[11] M. M. Murnane, H. C. Kapteyn, and R. W. Falcone, Appl. Phys. Lett. **56**, 1948 (1990).
[12] M. D. Duncan, R. Mahon, L. L. Tankersley, and J. Reintjes, Appl. Opt. **29**, 2369 (1990).
[13] R. Shepherd, R. Booth, D. Price, M. Bowers, D. Swan, J. Bonlie, B. Young, J. Dunn, B. White, and R. Stewart, Rev. Sci. Instrum. **66**, 719 (1995).
[14] Z. Chang, A. Rundquist, M. M. Murnane, H. C. Kapteyn, X. Liu, B. Shan, J. Liu, L. Niu, M. Gong, and X. Zhang, Appl. Phys. Lett. **69**, 133 (1996).
[15] A. Maksimchuk, M. Kim, J. Workman, G. Korn, J. Squier, D. Du, D. Umstadter, and G. Mourou, Rev. Sci. Instrum. **67**, 697 (1996).
[16] G. Mourou and S. Williamson, Appl. Phys. Lett. **41**, 44 (1982).
[17] S. Williamson, G. A. Mourou, and J. M. C. Li, Phys. Rev. Lett. **52**, 2364 (1984).
[18] H. E. Elsayed-Ali and G. A. Mourou, Appl. Phys. Lett. **52**, 103 (1988).
[19] H. E. Elsayed-Ali and J. W. Herman, Rev. Sci. Instrum. **61**, 1636 (1990).
[20] H. E. Elsayed-Ali and J. W. Herman, Appl. Phys. Lett. **57**, 1508 (1990).
[21] J. W. Herman and H. E. Elsayed-Ali, Phys. Rev. Lett. **68**, 2952 (1992).
[22] J. W. Herman and H. E. Elsayed-Ali, Phys. Rev. Lett. **69**, 1228 (1992).
[23] J. W. Herman, H. E. Elsayed-Ali, and E. A. Murphy, Phys. Rev. Lett. **71**, 400 (1993).
[24] J. W. Herman and H. E. Elsayed-Ali, Phys. Rev. B **49**, 4886 (1994).
[25] M. Aeschliman, E. Hull, J. Cao, C. A. Schmuttenmaer, L. G. Jahn, Y. Gao,

H. E. Elsayed-Ali, D. A. Mantell, and M. R. Scheinfein, Rev. Sci. Instrum. **66**, 1000 (1995).
[26] P. M. Weber, S. D. Carpenter, and T. Lucza, Proc. SPIE **2521**, 23 (1995).
[27] J. R. Thompson, P. M. Weber, and P. J. Estrup, Proc. SPIE **2521**, 113 (1995).
[28] H. E. Elsayed-Ali and P. M. Weber, in *Time-Resolved Diffraction*, edited by J. R. Helliwell and P. M. Rentzepis (Oxford University, Oxford, UK, 1997), Chap. 12, pp. 284–322.
[29] J. C. Williamson, J. Cao, H. Ihee, H. Frey, and A. H. Zewail, Nature (London) **386**, 159 (1997).
[30] H. Ihee, J. Cao, and A. H. Zewail, Chem. Phys. Lett. **281**, 10 (1997).
[31] J. Cao, H. Ihee, and A. H. Zewail, Chem. Phys. Lett. **290**, 1 (1998).
[32] M. Ya. Schelev, G. I. Bryukhnevich, V. I. Lozovoi, M. A. Monastyrski, A. M. Prokhorov, A. V. Smirnov, and N. S. Vorobiev, Opt. Eng. **37**, 2249 (1998).
[33] X. L. Zeng, B. Lin, I. El-Kholy, and H. E. Elsayed-Ali, Surf. Sci. **439**, 95 (1999).
[34] X. L. Zeng, B. Lin, I. El-Kholy, and H. E. Elsayed-Ali, Phys. Rev. B **59**, 14907 (1999).
[35] P. Kung, H. C. Lihn, and H. Wiedemann, Phys. Rev. Lett. **73**, 967 (1994).
[36] R. Clauberg and A. Blacha, J. Appl. Phys. **65**, 4095 (1989).
[37] J. P. Girardeau-Montaut and C. Girardeau-Montaut, J. Appl. Phys. **65**, 2889 (1989).
[38] C. Girardeau-Montaut, J. P. Girardeau-Montaut, and H. Leboutet, Appl. Phys. Lett. **55**, 2556 (1989).
[39] B.-L. Qian and H. E. Elsayed-Ali, J. Appl. Phys. (submitted).